Journal of Alloys and Compounds 509 (2011) 1060–1064

Contents lists available at ScienceDirect

Journal of Alloys and Compounds

journal homepage: www.elsevier.com/locate/jallcom

Enhanced magnetization and magnetoelectric coupling in hydrogen treated hexagonal $YMnO_3$

Nagesh Kumar[a], Anurag Gaur[b,*], G.D. Varma[a]

[a] Department of Physics, Indian Institute of Technology Roorkee, Roorkee-247667, India
[b] Department of Physics, National Institute of Technology, Kurukshetra-136119, India

ARTICLE INFO

Article history:
Received 8 May 2010
Received in revised form
26 September 2010
Accepted 28 September 2010
Available online 8 October 2010

PACS:
75.80.+q
77.80.−e
77.84.−s

Keywords:
Multiferroics
Magnetic properties
Ferroelectrics

ABSTRACT

The single phase hexagonal $YMnO_3$ has been synthesized via sol–gel route by adopting two different sintering conditions. In one case, sintering has been done at ~700 °C in Ar/H_2 atmosphere and in other case it has been done at ~1250 °C in air. Magnetic measurements of the samples, synthesized by sintering at relatively lower temperature in Ar/H_2 atmosphere, show the enhanced ferromagnetic behaviour at 10 K. *M–H* curve shows that the value of saturation magnetization (M_s) at 10 K is 8.04 emu/g for Ar/H_2 sintered sample while it is 2.93 emu/g for the air sintered sample. Moreover, a weak ferromagnetic signal at room temperature has been observed in $YMnO_3$ compound. Magnetization versus magnetic field (*M–H*) curves of hydrogen treated samples, measured at room temperature, show small kink in the linear variation near origin, possibly due to presence of weak ferromagnetic interactions in the samples at room temperature. However, the polarization–electric field (*P–E*) curve shows weak ferroelectric characteristics for the Ar/H_2 sintered samples. It is suggested that the enhanced ferromagnetism in Ar/H_2 sintered sample originates from the presence of oxygen vacancies in the Ar/H_2 sintered samples. Moreover, the magnetoelectric coupling coefficient at room temperature is improved to 106 mV/cm Oe for Ar/H_2 sintered sample as compared to 96 mV/cm Oe for air sintered sample at 40 kHz ac magnetic field frequency.

© 2010 Elsevier B.V. All rights reserved.

1. Introduction

The yttrium and rare-earth manganites $RMnO_3$ crystallize in two structural phases: the hexagonal phase for R = Ho, Er, Tm, Yb, Lu, or Y (with smaller ionic radii) and the orthorhombic phase for R = La, Ce, Pr, Nd, Sm, Eu, Gd, Tb, or Dy (with larger ionic radii) [1,2]. In these compounds, the angle Mn–O–Mn is close to 180°, facilitating magnetic ordering via an indirect exchange interaction between the Mn ions through the O ions. While magnetic ordering occurs in both hexagonal and orthorhombic manganites [3–5], ferroelectric ordering occurs only in the hexagonal [1], which belong to the non-centrosymmetric $P6_3cm$ space group. Therefore hexagonal yttrium form an interesting class of materials in which the ferroelectricity and magnetism coexist at low temperature and these kinds of materials are termed as multiferroics [6]. Multiferroics, sometimes called magnetoelectrics, are the materials that posses both ferroelectricity and ferromagnetism in the same phase [6–9]. These combined properties are thought to be nearly mutually exclusive. In fact, multiferroics are very few in existence. Hill [8] explored the fundamental physics behind the scarcity of the ferromagnetic ferroelectric coexistence. Because of their exclusive properties, these compounds present opportunities for potential applications in information storage process, spintronics, multi-state memories and magnetoelectric sensors [10–12]. The hexagonal $YMnO_3$ is the typical example of multiferroic that has the ferroelectric Curie temperature (T_C) near 900 K [13] and magnetic Neel temperature (T_N) below 70 K [14]. The lower T_N is a limitation for the multiferroic applications of $YMnO_3$, and it is an important issue to improve room temperature ferromagnetic properties of the present material. However, several efforts have been made to improve Neel temperature and magnetization in $YMnO_3$ by the doping of various ions on the Y and Mn site of $YMnO_3$ [15–21] but very few studies reported the enhanced magnetic behaviour in $YMnO_3$ [17,21]. Srivastava et al. [17] reported the weak ferromagnetic interaction in electron doped $Y_{1-x}Ce_xMnO_3$ (x = 0–0.10) due to double exchange interaction in Mn^{2+}–Mn^{3+} network while it has been found that the doping of Y on La site and Fe on Mn site of $LaMnO_3$ triggers antiferromagnetic interactions between Fe^{3+} and Mn^{4+} spins [20]. Furthermore, very recently Ma et al. [21] reported the weak ferromagnetic characteristics even up to room temperature in Fe doped $YMn_{0.8}Fe_{0.2}O_3$ compound. Most of the efforts are made to improve the magnetization by doping studies but very rare on pure $YMnO_3$. Interestingly, Ma et al. [22] reported the enhancement in magnetic

* Corresponding author. Tel.: +91 1744 233549; fax: +91 1744 238050.
E-mail addresses: anuragdph@gmail.com, gauranu791@rediffmail.com (A. Gaur).

0925-8388/$ – see front matter © 2010 Elsevier B.V. All rights reserved.
doi:10.1016/j.jallcom.2010.09.181

ordering in pure $YMnO_3$ by synthesizing through an in situ spark plasma sintering technique.

In the present work, we also try to improve the magnetization in pure $YMnO_3$ by sintering the material in reducing atmosphere of Ar (95%)/H_2 (5%). It has been found that by sintering $YMnO_3$ in Ar/H_2 atmosphere, not only magnetization is improved but magnetoelectric coupling is also enhanced. Furthermore, we get the hexagonal $YMnO_3$ phase at relatively lower sintering temperature (700 °C) for Ar/H_2 sintered sample as compared to the required 1250 °C sintering temperature for air atmosphere. However, a slight decrease in ferroelectric polarization is observed in the Ar/H_2 sintered samples.

2. Experimental procedures

The polycrystalline $YMnO_3$ samples were prepared by sol–gel method. The required amounts of high purity $Y(NO_3)_3{\cdot}5H_2O$ and $Mn(CH_3COO)_2{\cdot}4H_2O$ were dissolved in the double distilled water to form an aqueous solution. An equal amount of ethylene glycol was added to this solution with continuous stirring. This solution was then heated on a hot plate at temperature of ~60–80 °C till a dry thick sol was formed. This was further decomposed in an oven at a temperature of 250 °C to get the dry fluffy material. This obtained polymeric precursor was calcined at 700 °C for 15 h in furnace. Then resulting calcined powder was reground and pressed in the form of pellets. These pellets were sintered at different temperature and environments and the single phase hexagonal $YMnO_3$ was obtained for the pellets sintered at 1250 °C in air for 10 h and 700 °C in (95%)Ar/(5%)H_2 atmosphere for 1 h. Pellets sintered at 1250 °C in air for 10 h are referred to as sample YMO-Air and sintered at 700 °C in (95%)Ar/(5%)H_2 atmosphere for 1 h are referred to as sample YMO-Ar/H_2. Furthermore, it is also noticed that increasing the sintering time (>1 h) for Ar/H_2 sintered sample deteriorate the hexagonal phase.

The structural characterization is done at room temperature by using X-ray diffraction (Bruker AXS D8 advance, Cu Kα radiation) technique. The microstructure of the samples is examined with FE-SEM (FEI, Quanta 200 F, Netherlands). The elemental analysis of the sintered samples is carried out using energy dispersive X-ray analyzer (EDAX' TSL, AMETEK) coupled with FE-SEM. Magnetization measurements are carried out by using SQUID magnetometer (SQUID–Quantum Design MPMS XL) and ferroelectric hysteresis loops are measured by using ferroelectric loop tracer.

3. Results and discussion

Fig. 1 shows the room temperature X-ray diffraction patterns using Cu Kα radiation. The XRD results reveal that both the samples (YMO-Air and YMO-Ar/H_2) have pure hexagonal phase and there is no sign of MnO_2 (which usually forms at synthesis temperature above 1100 °C) or orthorhombic $YMnO_3$ (which appears at high pressures). The high intensity of XRD peaks for the sample YMO-Air as compared to the sample YMO-Ar/H_2 indicates the better crystallinity of the earlier sample. It is also found that the peak width of sample YMO-Ar/H_2 (sintered at 700 °C) is larger than the sample YMO-Air (sintered at 1250 °C), which indicates that the particle size of the sample YMO-Ar/H_2 is smaller than the sample YMO-Air. The particle size estimated from X-ray data using Scherrer's formula

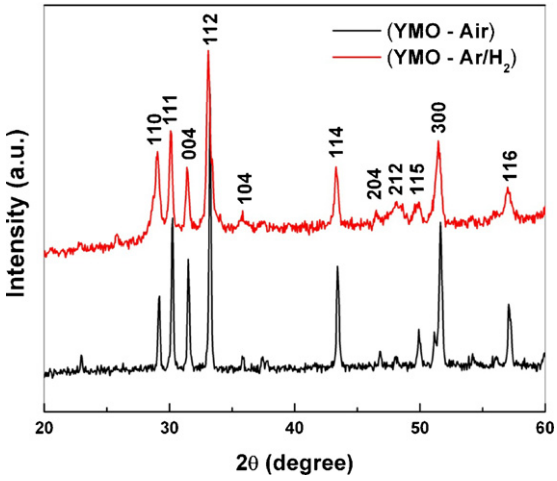

Fig. 1. X-ray diffraction patterns of YMO-Air and YMO-Ar/H_2 samples.

(PS ~ $K\lambda/\beta\cos\theta$ where $k \sim 0.89$ is the shape factor, λ is wavelength of X-rays, β is the FWHM and θ is the Bragg angle) is 30 nm for YMO-Ar/H_2 sample and 400 nm for sample YMO-Air. A minor shift in the Bragg peaks of YMO-Ar/H_2 sample with respect to YMO-Air sample towards lower Bragg angle indicates a minor expansion in unit cell. The calculated lattice parameters (a and c for hexagonal phase with space group $P6_3cm$) are $a = 6.141$ Å and $c = 11.404$ Å for YMO-Ar/H_2 sample and $a = 6.136$ Å and $c = 11.398$ Å for YMO-Air sample. This slight expansion in unit cell of YMO-Ar/H_2 sample may be due to presence of oxygen vacancies in this hydrogen treated sample as being confirmed ahead by EDX results.

The FESEM images of both the samples (YMO-Air and YMO-Ar/H_2) are shown in Fig. 2. FESEM images show that the morphology of the sample YMO-Air is dense and uniform while that of the sample YMO-Ar/H_2 shows grains of smaller size with some pores and poor density, which may be due to presence of oxygen vacancies. The reduction in grain size by hydrogenation process can be clearly noticed by FESEM images. The grain size calculated from FESEM images for Ar/H_2 sintered sample is ~70 nm as compared to 800 nm for air sintered sample. However, both XRD and FESEM results show the reduction in particle/grain size for Ar/H_2 sintered sample but there is a difference between particle size calculated through XRD and grain size calculated through FESEM. This difference is due to the fact that grains are composed of several particles, which may introduce the internal stress or defects in the structure. The EDX results show that the Y/Mn atomic ratio for the sample YMO-Ar/H_2 is close to 1 but the oxygen content is found nearly

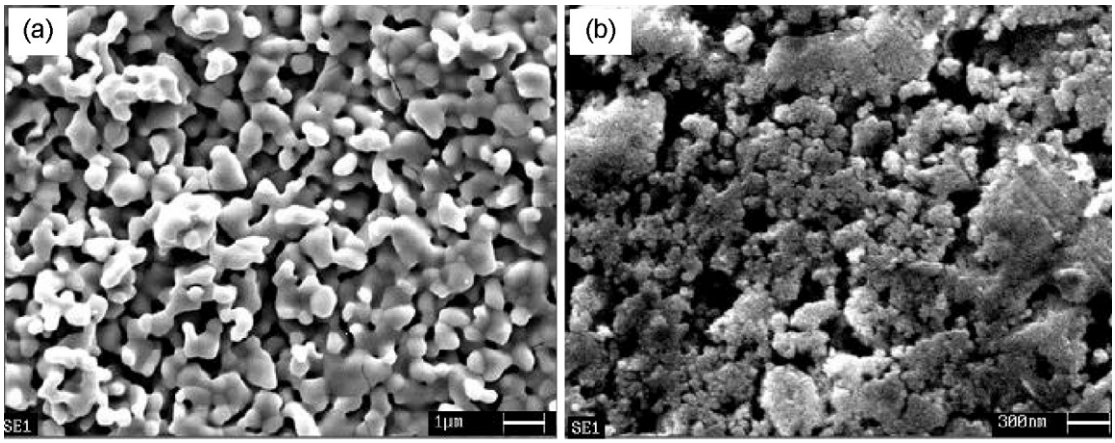

Fig. 2. Field emission scanning electron micrographs of (a) YMO-Air and (b) YMO-Ar/H_2 samples.

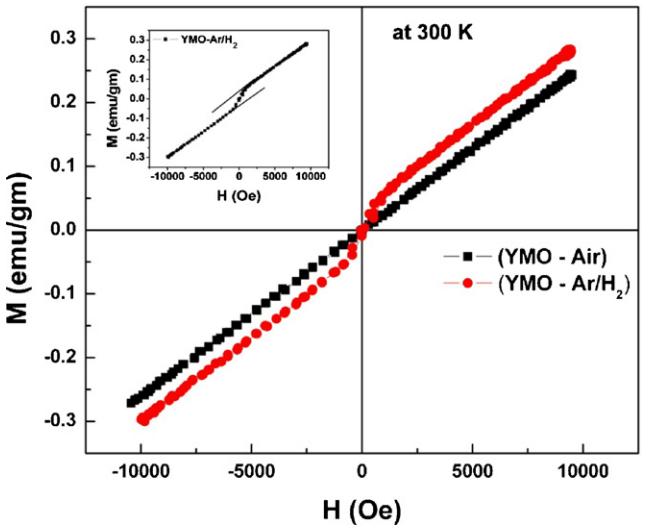

Fig. 3. Magnetization versus magnetic field (M–H) curves of YMO-Air and YMO-Ar/H_2 samples measured at room temperature. Inset shows the ferromagnetic kink near origin in YMO-Ar/H_2 sample.

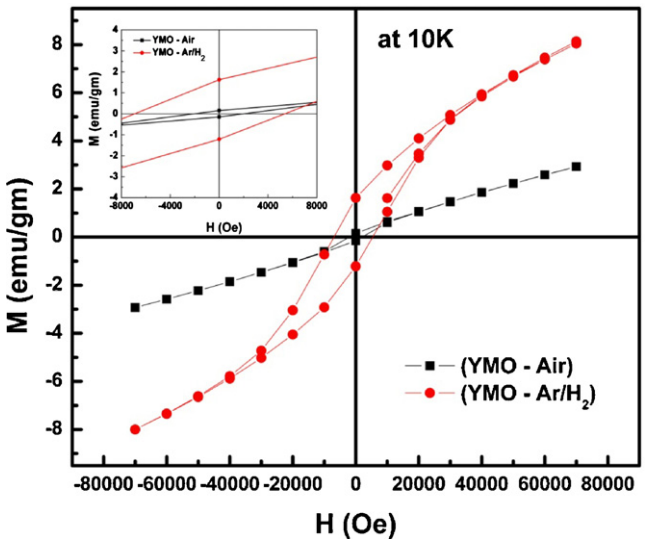

Fig. 4. Magnetization versus magnetic field (M–H) curves of YMO-Air and YMO-Ar/H_2 samples measured at 10 K. Inset shows the enlarge view of M–H curve at low fields.

2.85 (instead of 3) whereas the oxygen content is close to 3 for the air sintered sample YMO-Air. Therefore, EDX results also indicate that the oxygen vacancies are produced in the YMO-Ar/H_2 sample through hydrogenation.

The magnetizations versus magnetic field (M–H) curves recorded at room temperature are shown in Fig. 3. The M–H curve of the sample YMO-Air shows linear variation of magnetization with magnetic field, suggesting paramagnetic behaviour of this sample. On the other hand, the M–H curve of sample YMO-Ar/H_2, measured at room temperature, shows a kink in the linear variation near origin, indicating some ferromagnetic fraction in this sample. Furthermore, the value of magnetization is also larger in the hydrogenated YMO-Ar/H_2 sample as compared to sample YMO-Air. The values of magnetization at room temperature are 0.24 and 0.28 emu/g for the sample YMO-Air and YMO-Ar/H_2, respectively. The non-linear behaviour (with ferromagnetic kink) in the YMO-Ar/H_2 sample has been shown clearly in the inset of Fig. 3.

We have also recorded M–H curves at 10 K for both the YMO-Air and YMO-Ar/H_2 samples. The magnetizations versus magnetic field (M–H) curves, recorded at 10 K, are shown in Fig. 4. The values of saturation magnetization (M_S) at 10 K are 2.93 and 8.04 emu/g for the YMO-Air and YMO-Ar/H_2 samples, respectively. This shows that the hydrogenated YMO-Ar/H_2 sample has larger value of magnetization as compared to sample YMO-Air. This indicates that the hydrogenation process helps in the enhancement of magnetization. However, a weak ferromagnetic signal is also observed in YMO-Air sample at 10 K (as shown in the inset of Fig. 4) but YMO-Ar/H_2 sample has clear hystresis phenomenon with a greater value of spontaneous magnetization. The value of spontaneous magnetization is 1.62 emu/g in YMO-Ar/H_2 sample while it is only 0.154 emu/g in YMO-Air sample. However, in spite of larger spontaneous magnetization in YMO-Ar/H_2 sample, it does not get saturation magnetization up to 80 kOe magnetic field, which indicates that still paramagnetic phase is dominating in the sample. This weak ferromagnetism, observed in hydrogenated $YMnO_3$, is believed to be Dzialoshinkii-Moriya type [23], and its origin is associated with the antisymmetric part of the anisotropic superexchange interaction. However, the exact mechanism for this enhanced ferromagnetic behaviour in the Ar/H_2 treated samples is not clear but experimental results of the present investigation, suggest that the presence of oxygen vacancies in the hydrogenated sample may also be responsible for this observed enhancement in

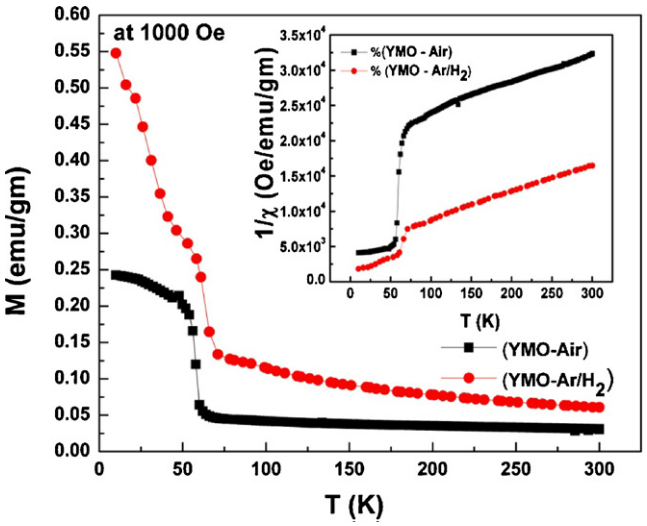

Fig. 5. Magnetization versus temperature (M–T) curves of YMO-Air and YMO-Ar/H_2 samples at 1000 Oe. Inset shows the reciprocal susceptibility versus temperature curve.

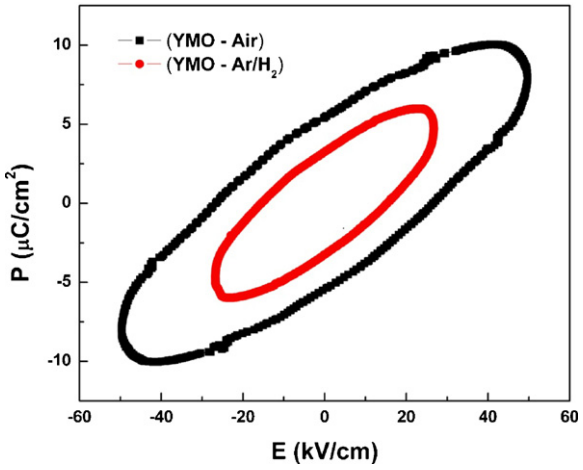

Fig. 6. Polarization versus electric field (P–E) hysteresis curves of YMO-Air and YMO-Ar/H_2 samples measured at room temperature.

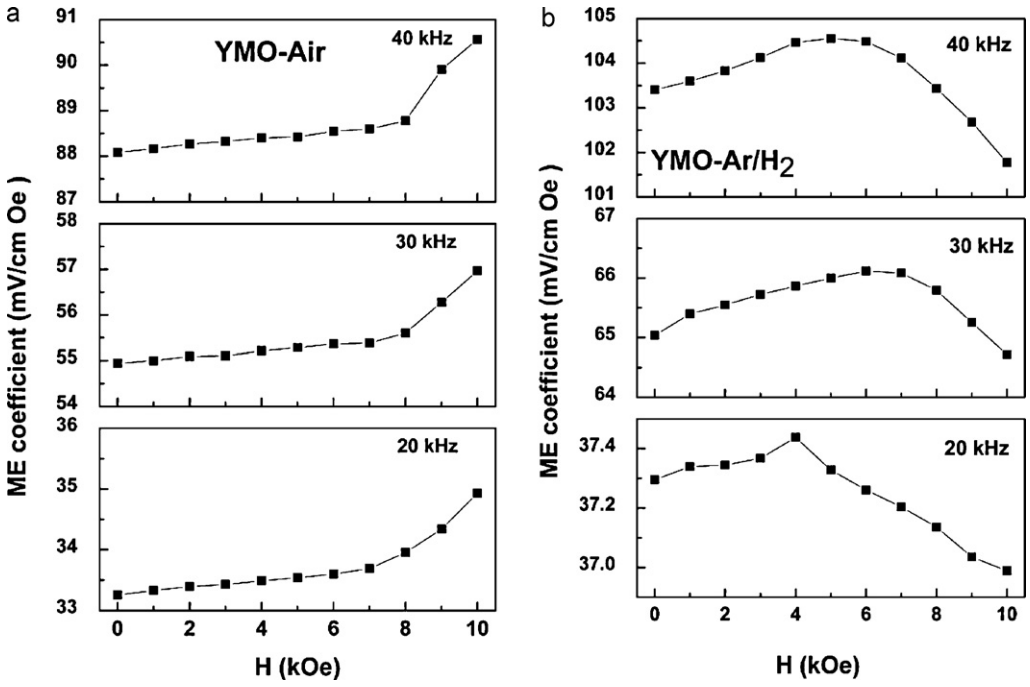

Fig. 7. Magnetoelectric (ME) coefficient (α_E) versus dc bias magnetic field (H_{Bias}) curve at room temperature for (a) YMO-Air and (b) YMO-Ar/H_2 at various ac magnetic field frequencies.

ferromagnetic behaviour. It has been reported by several groups that additional charge carriers created by oxygen vacancies play a crucial role in enhancing the ferromagnetism, most likely in mediating the exchange interactions [24–27] between Mn ions. Moreover, in our earlier work, we also found enhancement in ferromagnetism of ZnO due to oxygen vacancies [28].

The magnetization versus temperature (M–T) curve, measured in 1000 Oe field in the temperature range of 80–300 K, is shown in Fig. 5. This also shows that the value of magnetization of hydrogenated sample YMO-Ar/H_2 is larger as compared to sample YMO-Air. Both the samples undergo a sharp paramagnetic to ferromagnetic transition (T_C) almost at the same temperature ~64 K, which is close to the reported value ~70 K by other groups [14]. The reciprocal susceptibility with temperature for both the samples has shown in the inset of Fig. 5. It shows the linear dependence above 70 K, which reveals the Curie–Weiss behaviour of paramagnetism. However, in the magnetic susceptibility of both the samples, no anomalies are observed, although there is a notable increase below 100 K. Moreover, the susceptibility for YMO-Air sample is saturated at low temperature around 60 K but it continuously increases for YMO-Ar/H_2 with decreasing the temperature, which also suggests larger magnetization in hydrogenated YMO-Ar/H_2 sample.

The ferroelectric characteristics of both the samples (YMO-Air and YMO-Ar/H_2) measured at room temperature, are shown in Fig. 6. No saturation in polarization electric field (P–E) curve is found for both ceramics up to maximum applied electric field due to poor leakage behaviours. Another observation from the hysteresis loops is that for both ceramics, further increase in the electric field will lead to electric breakdown. The YMO-Ar/H_2 sample has lower value of polarization and get electric breakdown at low electric field. The restriction of higher field in Ar/H_2 sintered $YMnO_3$ is due to low resistivity associated with motion of oxygen vacancies.

The coexistence of the ferroelectric and ferromagnetic phases in the present samples gives rise to a ME effect, which is characterized by the magnetoelectric voltage coefficient $\alpha_E = dE/dH$. The variations in magnetoelectric (ME) coefficient with H_{Bias} at various ac magnetic field frequencies are shown in Fig. 7. It can be observed from Fig. 7(a) that the α_E for sample YMO-Air increases very slowly with increasing H_{Bias} from zero to 7 kOe and starts to increase sharply above 7 kOe. However, the α_E of YMO-Ar/H_2 firstly increases and then starts to decrease at a particular value of H_{Bias} (as shown in Fig. 7(b)). This transition is shifting towards higher dc bias magnetic field with increasing the frequency. Furthermore, it has been found that the sample YMO-Ar/H_2 has the larger value of α_E as compared to YMO-air sample at all frequencies. This indicates that the magnetoelectric coupling improves in YMO-Ar/H_2 samples through hydrogen treatment. The maximum value of α_E is found to be 106 mV/cm Oe for YMO-Ar/H_2 sample while it is 96 mV/cm Oe for YMO-Air sample at 40 kHz frequency. The overall increase in the value of α_E for YMO-Ar/H_2 is because of its enhanced magnetization behaviour (as shown in Fig. 4) and the decrease in value of α_E at a particular H_{Bias} may be because of its reduced ferroelectric behaviour (as shown in Fig. 6). In addition, an overall α_E increase for both the samples is observed with increasing frequency from 20 to 40 kHz. The increase in α_E value with frequency is most likely due to the frequency dependence of the dielectric constant and piezoelectric coefficient of $YMnO_3$.

4. Conclusions

In summary, we synthesized single hexagonal $YMnO_3$ phase at 700 °C and 1250 °C by sintering in Ar/H_2 and air atmospheres, respectively. The magnetic measurements show enhanced magnetization in hydrogenated YMO-Ar/H_2 sample as compared to the air sintered sample. It is argued that oxygen vacancies are responsible for ferromagnetic ordering to enhance magnetization. However, both ceramics show weak ferroelectric characteristics at room temperature but magnetoelectric coupling is improved for Ar/H_2 sintered samples.

Acknowledgements

The authors are grateful to Prof. O.N. Srivastava (B.H.U.), Prof. D. Pandey (B.H.U.) for encouragements and helpful discussions. The

authors are also grateful to Dr. K.L. Yadav (I.I.T.R.) to provide facility for *P–E* measurements.

References

[1] F. Bertant, F. Forrat, P. Fang, C. R. Acad. Sci. 256 (1963) 1958.
[2] L. Martın-Carron, A. de Andres, M.J. Martınez-Lope, M.T. Casais, J.A. Alonso, J. Alloys Compd. 323–324 (2001) 494.
[3] W.C. Kochler, H.L. Yakel, E.O. Wollan, J.W. Cable, Phys. Lett. 9 (1964) 93.
[4] R. Pauthenet, C. Veyret, J. Phys. (France) 31 (1970) 65.
[5] V.E. Wood, A.E. Austin, E.W. Collings, K.C. Brog, J. Phys. Chem. Solids 34 (1973) 857.
[6] G.A. Smolenskii, I.E. Chupis, Sov. Phys. Usp. 25 (1982) 475.
[7] H. Schmid, Ferroelectrics 162 (1994) 317.
[8] N.A. Hill, J. Phys. Chem. B 104 (2000) 6694.
[9] S. Chena, L. Wang, H. Xuan, Y. Zheng, D. Wang, J. Wu, Y. Du, Z. Huang, J. Alloys Compd. 506 (2010) 537.
[10] M. Fiebig, J. Phys. D: Appl. Phys. 38 (2005) R123.
[11] W. Prellier, M.P. Singh, P. Murugavel, J. Phys: Conden. Matter. 17 (2005) R803.
[12] C. Ederer, N. Spaldin, Phys. Rev. B 71 (2005) 060401.
[13] T. Lonkai, D.G. Tomuta, U. Amann, J. Ihringer, R.W.A. Hendrikx, D.M. Tobbens, J.A. Mydosh, Phys. Rev. B 69 (2004) 134108.
[14] T. Katsufuji, S. Mori, M. Masaki, Y. Moritomo, N. Yamamoto, H. Takagi, Phys. Rev. B 64 (2001) 104419.
[15] A. Nugroho, N. Bellido, U. Adem, G. Nénert, C. Simon, M.O. Tjia, M. Mostovoy, T.T.M. Palstra, Phys. Rev. B 75 (2007) 174435.
[16] S.L. Samal, W. Green, S.E. Lofland, K.V. Ramanujachary, D. Das, A.K. Ganguli, J. Solid State Chem. 181 (2008) 61.
[17] S.K. Srivastava, M. Kar, S. Ravi, P.K. Mishra, P.D. Babu, J. Magn. Magn. Mater. 320 (2008) 2382.
[18] A.E. Smith, H. Mizoguchi, K. Delaney, N.A. Spaldin, A.W. Sleight, M.A. Subramanian, J. Am. Ceram. Soc. 131 (2009) 17084.
[19] A. Dixit, E. Andrew, M.A. Smith, G. Subramanian, Lawes, Solid State Commun. 150 (2010) 746.
[20] N. Kallel, S.B. Abdelkhalek, S. Kallel, O. Pena, M. Oumezzine, J. Alloys Compd. 501 (2010) 30.
[21] Y. Ma, X.M. Chen, Y.J. Wu, Y.Q. Lin, Ceram. Int. 36 (2010) 727.
[22] Y. Ma, Y.J. Wu, X.M. Chen, J.P. Cheng, Y.Q. Lin, Ceram. Int. 35 (2009) 3051.
[23] I. Dzialoshinskii, J. Phys. Chem. Solids 4 (1958) 241; T. Moriya, Phys. Rev. 120 (1960) 91.
[24] D.J. Priour, E.H. Hwang, S.D. Sarma, Phys. Rev. Lett. 92 (2004) 117201.
[25] A. Quesada, M.A. Garcia, P. Crespo, A. Hernando, J. Magn. Magn. Mater. 304 (2006) 75.
[26] C. Ederer, N.A. Spaldin, Phys. Rev. B 71 (2005) 224103.
[27] H.S. Hsu, J.C.A. Huang, Appl. Phys. Lett. 88 (2006) 242507.
[28] V.K. Sharma, G.D. Varma, J. Appl. Phys. 102 (2007) 056105.